Electronic structure of the Cu_2MnAl Heusler alloy

2000 J. Phys.: Condens. Matter 12 2997

(http://iopscience.iop.org/0953-8984/12/13/310)

J. Phys.: Condens. Matter **12** (2000) 2997–3012. Printed in the UK PII: S0953-8984(00)08613-6

Electronic structure of the Cu_2MnAl Heusler alloy

Aniruddha Deb† and Yoshiharu Sakurai

Japan Synchrotron Radiation Research Institute (JASRI), SPring-8, Mikazuki, Sayo, Hyogo 679-5198, Japan

E-mail: ani12@spring8.or.jp

Received 11 October 1999

Abstract. The electronic structure and chemical bonding mechanism of the Heusler alloy Cu_2MnAl are studied on the basis of band-structure calculations, using the full-potential linearized augmented-plane-wave (FLAPW) method. The calculations are performed within both the local spin-density approximation (LSDA) and the generalized gradient approximation (GGA). The calculated band structures and the densities of states within the GGA are compared with the earlier-reported experimental results of ultraviolet photoemission spectroscopy. The comparisons support the physical picture proposed by Kübler and co-workers, in which the occupied d states of Mn are delocalized by their strong interaction with the d states of Cu. The magnetic Compton profiles (MCPs) are also calculated and compared with the earlier-reported experimental results. The comparisons show that the GGA is better able to reproduce the experimental profiles than the LSDA. The spin moment on the Mn site is calculated to be 3.20 μ_B, which is in agreement with the value deduced from the experimental profiles.

1. Introduction

Heusler alloys are ternary intermetallic compounds with stoichiometric composition X_2YZ, where X can be a 3d, 4d or 5d element (X = Co, Ni, Cu, Pd etc); Y = Mn and Z = Al, Sn, In, Sb, Si, Ga, Ge or As. The Heusler alloy structure is illustrated in figure 1. The structure is face-centred cubic, having space group $Fm3m$. There are four Cu_2MnAl molecules per unit cell. Cu atoms reside at (1/4, 1/4, 1/4) and (3/4, 3/4, 3/4), Mn at (1/2, 1/2, 1/2) and Al at

† Author to whom any correspondence should be addressed: Japan Synchrotron Radiation Research Institute (JASRI), SPring-8, 323-3, Mihara, Mikazuki, Sayo, Hyogo 679-5198, Japan. Fax: +81-(0)7915-8-0830.

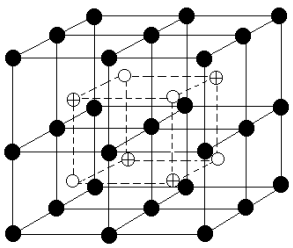

Figure 1. The stoichiometric Cu_2MnAl unit cell, showing the four interpenetrating fcc sublattices. Cu atoms occupy (1/4, 1/4, 1/4) and (3/4, 3/4, 3/4) positions. Mn atoms are at (1/2, 1/2, 1/2) and Al at (0, 0, 0). Cu: solid black circles; Mn: crossed circles; Al: open circles.

(0, 0, 0) [1]. Heusler alloys are interesting magnetic systems because they possess localized magnetic moments although they are all metallic. The magnetic properties in these systems are known to be strongly dependent on both the conduction electron concentration [2] and the chemical order [3]. Cu_2MnAl is a ferromagnetic Heusler alloy with a Curie temperature, lattice constant and saturation moment of 603 K, 0.5949 nm and 4.12 μ_B respectively [4]. Detailed studies have been performed on the magnetic, electrical and structural properties of Cu_2MnAl [5–8]. However, the formation and coupling of the magnetic moments in Mn-related Heusler alloys are still the subject of theoretical and experimental investigations.

It is well established, by the neutron diffraction technique, that the magnetic moment of Cu_2MnAl can be solely attributed to the Mn atoms [9]. A number of neutron diffraction experiments concluded that the 3d electrons are well localized on the Mn atoms, while the RKKY-type s–d interactions are of long range, extending to more than eight neighbours [10–12]. These experimental findings were compared with a number of theoretical band-structure calculations [13–19]. Kübler *et al* [18], carrying out self-consistent spin-polarized energy band calculations, indicated that there is no significant direct interaction between the d electrons of different Mn atoms, but the occupied d states of Mn are delocalized by their strong interaction with the Cu d states. Williams *et al* [17], studying the magnetic properties of Heusler alloys, showed that there were no spin-down 3d electrons on the Mn site, which resulted in a magnetic moment on the Mn site. Furthermore, Kübler [15] made a theoretical study of transition metal alloys including itinerant ferromagnetism and concluded that the role of the Cu atom in the Cu_2MnAl Heusler alloy is limited to the determination of the lattice constant only.

These physical pictures obtained from the experiments and the theoretical calculations were recently examined utilizing the magnetic Compton scattering technique by Zukowski *et al* [20]. Using 92 keV circularly polarized synchrotron radiation, they found that the conduction electrons have a negative spin polarization of 0.4 μ_B, which is in reasonable agreement with the theoretical prediction of Ishida *et al* [19], but disagrees with the neutron scattering experiment findings [21]. They also pointed out that there was no 3d spin moment at the Cu site, while that of the Mn site is 3.25 μ_B, which is consistent with the neutron experiment but disagrees with the theoretical calculation. The ultraviolet photoemission spectrum of Cu_2MnAl Heusler alloy has been obtained by Brown *et al* [22]. The measured spectrum reveals that the Mn 3d character extends across the full width of the valence bands. Comparison between the experiment and the calculation using the symmetrized augmented-plane-wave method [13] shows a significant difference around 1.5 eV binding energy, for which the calculation predicts a peak due to both Cu and Mn states while no peak is observed in the experimental spectrum.

There is no consistent agreement between the reported experiments and the band theoretical calculations, which motivated new band-structure calculations within the local spin-density approximation (LSDA) and generalized gradient approximation (GGA). The LSDA is a powerful theoretical tool, but it is unable to account for non-local contributions to the exchange–correlation effects [23]. In electronic calculations, several attempts and suggestions for going beyond the LSDA have been studied [24]. Over the past few years the GGA especially has attracted wide interest [25]. The GGA goes beyond the LSDA by including the first derivative of the electron density in the exchange and correlation energy functional. The GGA is able to improve the description of some of the cohesive properties compared to the LSDA [26], although a general improvement in other systems has not been obtained yet (see reference [27]). An example in which the GGA provides a significant improvement over the LSDA is the H_2 dissociation on the Cu(111) surface [28]. It has also been showed that the GGA gives results in better agreement with the experiments than the LSDA for finite systems (atoms and molecules)

and for metallic surfaces [29, 30]. One reason for this is that the interactions in these systems are related to the tails of the electronic wavefunctions, for which the GGA should, in principle, give a better description than the LSDA. Furthermore, a study of the LSDA and GGA has recently been made for s–p materials by Lee and Martin [31], and for 3d and 4d transition metals by Kokko and Das [32]. In the former case their calculations of the atomic total energy and the first ionization energy with the GGA functional were more accurate than those with the LSDA, while in the latter case systematic improvements of the results were obtained in comparison with those obtained using the LSDA.

This paper is organized as follows. In section 2, we describe the calculation of the band structure. Then we present the density of states in section 3 and the electron densities in section 4. The Compton profiles are analysed in section 5, while discussion and conclusions are given in section 6.

2. Band-structure calculations

Self-consistent band-structure calculations were carried out using the scalar-relativistic full-potential linearized augmented-plane-wave (FLAPW) method [23]. The exchange–correlation functional was taken within the LSDA as well as within the GGA. In the former case we applied the Perdew and Wang parametrization [33], while for the latter we applied the Perdew *et al* [30] parametrization.

In the present calculations, the origin of the cell was chosen to be at the aluminium site, in order for there to be inversion symmetry, which allowed us to have all matrix elements real. In the calculations we have distinguished between the inner-shell electrons from Cu, Mn 1s, 2s, 2p and Al 1s, 2s and the valence band electrons from the Cu, Mn, 3d, 4s, 4p and Al 3s, 3p, 3d shells. The extended Cu, Mn 3s, 3p states and Al 2p states were handled separately as semi-core bands. To provide a concise picture of this system we will present here our theoretical results utilizing the GGA scheme, and for a comparative study of our calculated results we have presented our LSDA results in some cases only.

A total of 15 iterations were necessary to achieve self-consistency, where the eigenvalues of the last two iterations differ by less than 0.1 mRyd. The FLAPW energy bands along the high-symmetry lines in the fcc Brillouin zone for the majority and minority spins are shown in figures 2 and 3, where the GGA and LSDA bands are shown by solid and dotted lines, respectively. Here the valence band has a bandwidth of 10.6 eV. The lowest band is of Al 3s character along with contributions from Cu and Mn 4s states. An analysis of the eigenvectors allows us to extract information about the character of the bands. The main results of this analysis are displayed in figures 4(a)–4(d), where the symbol size is proportional to the strength of the orbital character of the bands. An analysis of these figures reveals that the Mn d minority-spin states are almost excluded from the Cu d minority-spin states, whereas the Mn d majority-spin states join with the Cu d majority-spin states. This is consistent with the previous calculation by Kübler *et al* [18], which can explain the localized magnetic moment as arising from diffuse (itinerant) electrons.

From the figures it is also evident that the Cu 3d state for the majority and minority spins is mainly confined to the 2–6 eV region of the valence band, while the main contribution of the Mn 3d majority spin is around 2 eV in the valence band. The lower conduction bands (within 3 eV above the Fermi level) are made from Mn 3d orbitals of the minority spin. Furthermore, our Mn 3d moment and Cu 3d moment calculated theoretically utilizing the GGA and LSDA schemes along with the earlier-reported experimental results are shown in table 1. From the table it is evident that our values calculated within the GGA scheme agree well with the experimental values reported by Zukowski *et al* [20]. Bozorth [34] and Dunlap

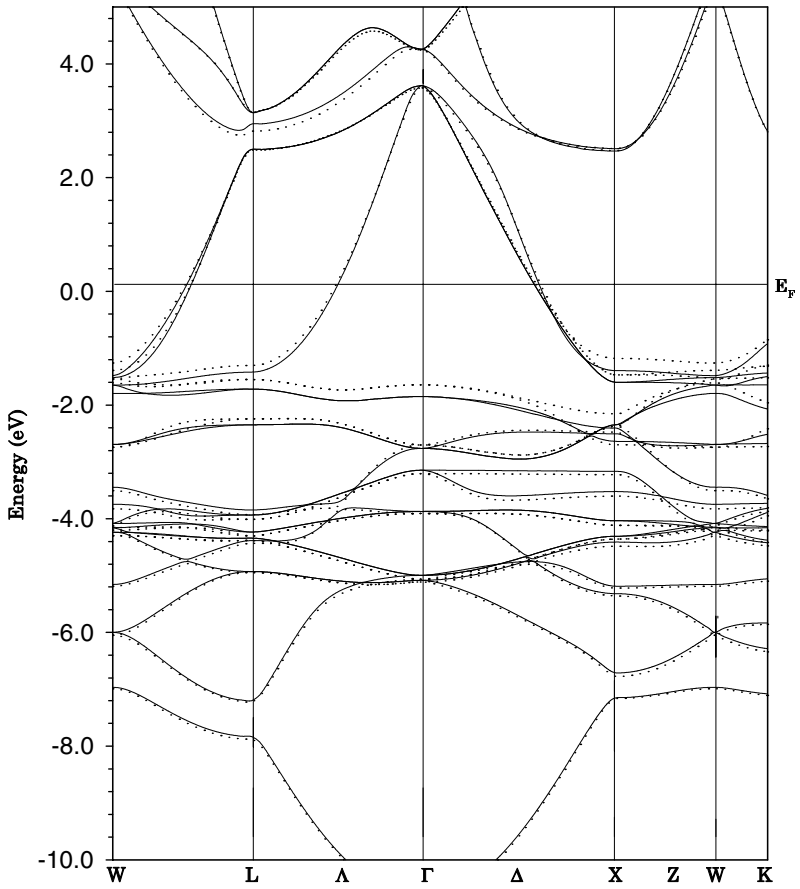

Figure 2. The FLAPW band structures of ferromagnetic Cu_2MnAl along the high-symmetry lines for the majority spin. The solid curves represent the GGA bands while the dotted curves represent the LSDA bands.

et al [35] found the saturation magnetization of Cu_2MnAl at room temperature to be 2.81 μ_B, while Endo *et al* [36] making a similar study on Cu_2MnAl reported a value of 3.37 μ_B as the saturation moment. It is important to note here that the p–d hybridization of the Mn 3d electrons with the Al p electrons has resulted in a magnetic moment per Mn atom less than 4 μ_B (table 1), which is a substantial reduction on the free-atom moment of 5 μ_B.

Table 1. Spin moments and total energy in Cu_2MnAl calculated utilizing the FLAPW–GGA and FLAPW–LSDA schemes.

Mn 3d moment (μ_B)			Cu 3d moment (μ_B)		
Mode of calculation		Experiment, Zukowski *et al*	Mode of calculation		Experiment, Zukowski *et al*
GGA	LSDA	[19]	GGA	LSDA	[19]
3.20	3.40	3.25	−0.04	−0.09	$<$ |0.05|
Total energy (Ryd/atom)			FLAPW–GGA		−9425.560 054
			FLAPW–LSDA		−9406.810 153

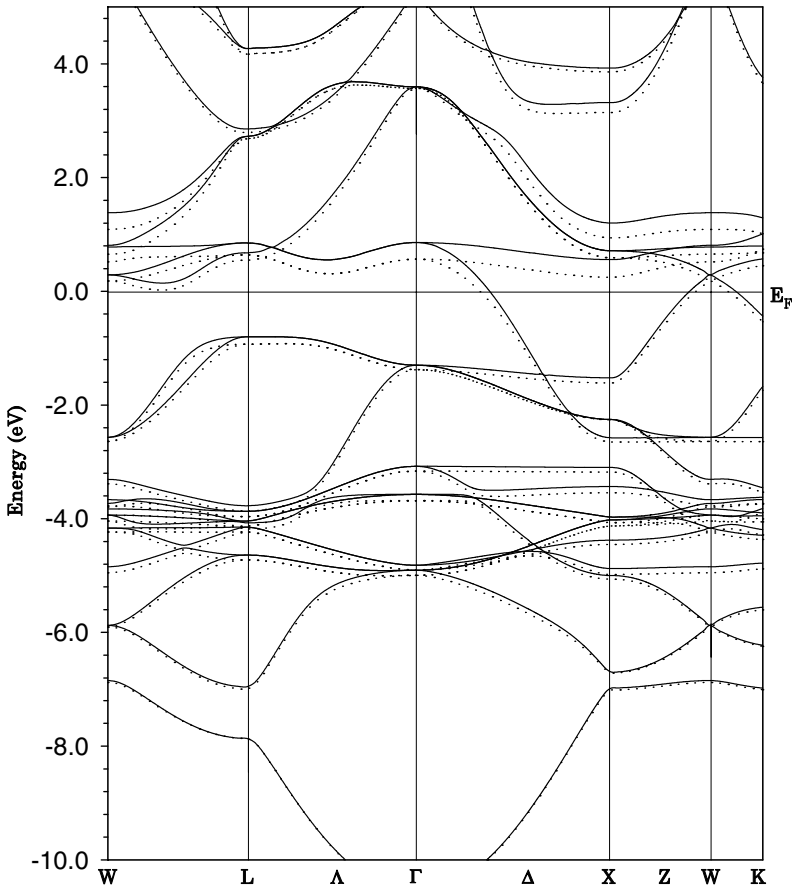

Figure 3. The FLAPW band structures of ferromagnetic Cu_2MnAl along the high-symmetry lines for the minority spin. The solid curves represent the GGA bands while the dotted curves represent the LSDA bands.

Hyperfine parameters such as the hyperfine field (HFF) provide information about the interaction of a nucleus with the surrounding charge distribution. It can be measured by various techniques like Mössbauer spectroscopy, nuclear magnetic resonance or perturbed angular correlation. The total hyperfine field (HFF) can be decomposed into three terms such as a dominant Fermi contact term, a dipolar term and an orbital contribution. We consider only the contact term, which in the scalar-relativistic limit is derived from the spin densities at the nuclear site:

$$H_c = \frac{8}{3}\pi\mu_B^2[\rho_\uparrow(0) - \rho_\downarrow(0)] \tag{1}$$

while in the fully relativistic case this spin density at the nucleus is replaced by its average over the Thomson radius $r_T = Ze^2/mc^2$ [37]. The hyperfine field calculated here under the GGA and the LSDA scheme for Cu, Mn and Al atoms in Cu_2MnAl Heusler alloys are given in table 2.

In order to understand the origin of the hyperfine field the site-projected valence electron contribution as well as the core contributions are also given in this table. Because of the opposite signs of the contributions from the core and valence electrons, the absolute value of

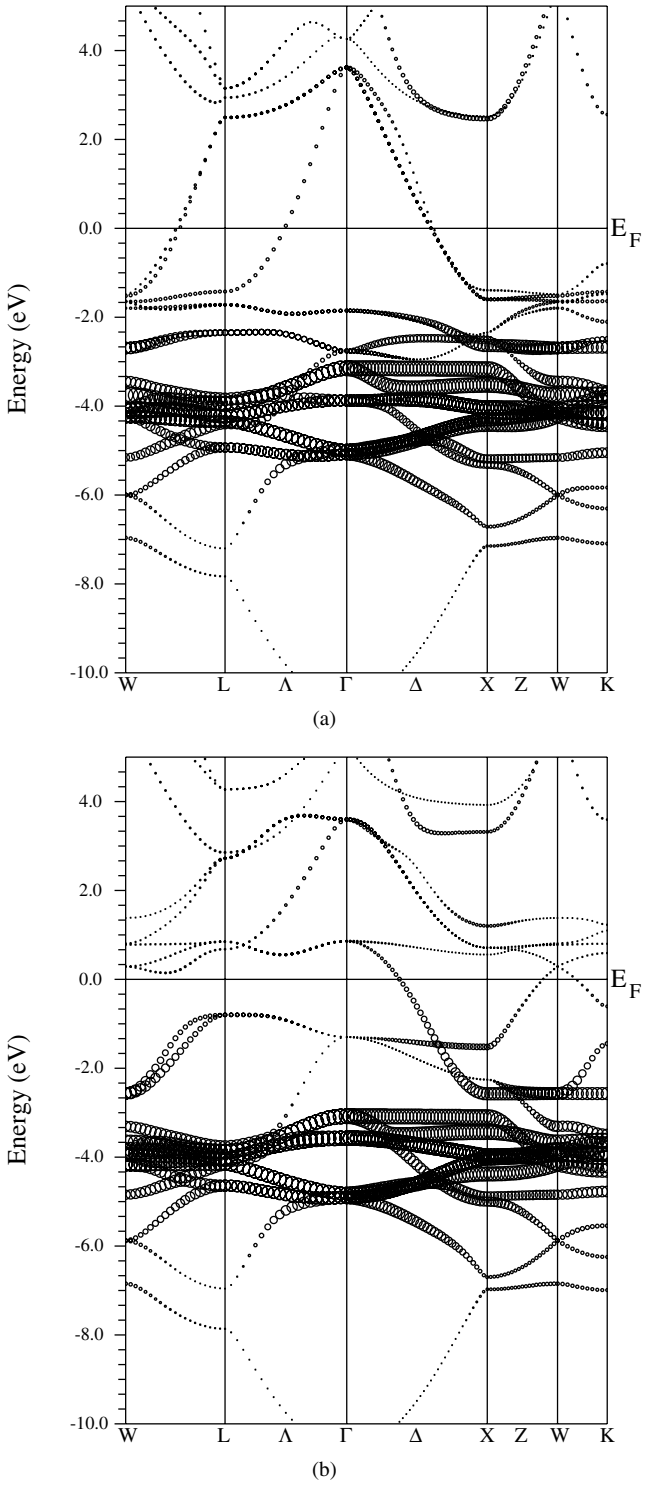

Figure 4. The GGA–FLAPW band-structure-character plots for ferromagnetic Cu_2MnAl: (a) the Cu 3d majority spin; (b) the Cu 3d minority spin; (c) the Mn 3d majority spin; (d) the Mn 3d minority spin. The symbol size indicates the strength of the orbital character of the bands.

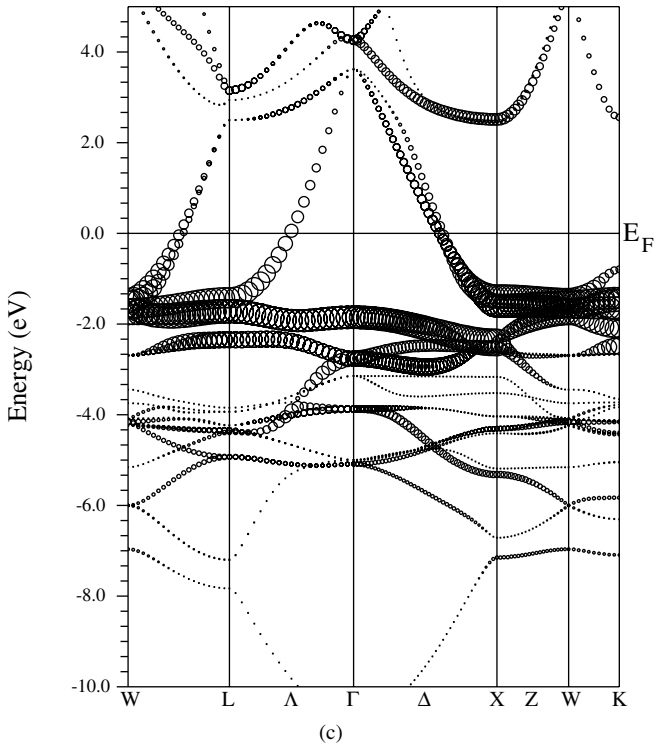

(c)

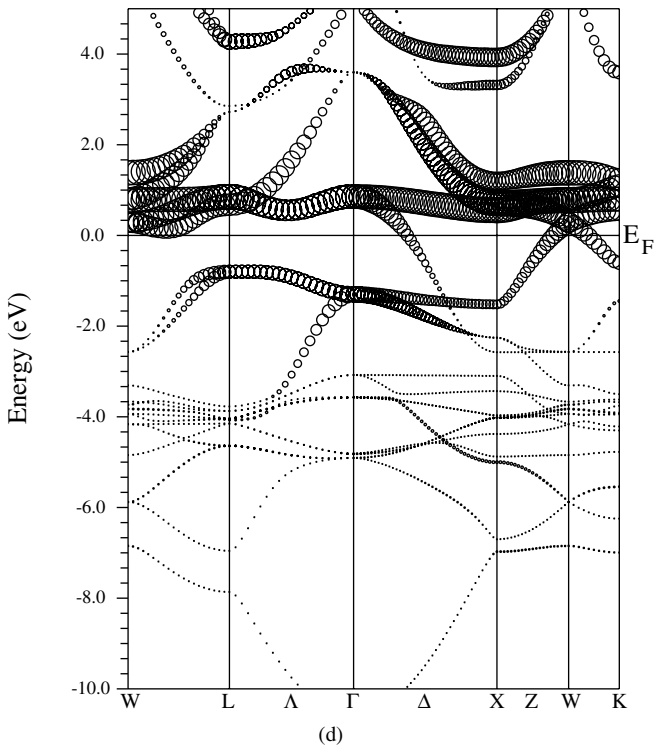

(d)

Figure 4. (Continued)

Table 2. Hyperfine fields of copper, manganese and aluminium in Cu_2MnAl.

Mode of calculation	Cu (kG)			Mn (kG)			Al (kG)		
	Valence	Core	Total	Valence	Core	Total	Valence	Core	Total
GGA	−220.3	−12.3	−232.6	330.3	−341.5	−11.2	−34.6	0.4	−34.2
LSDA	−230.6	−15.4	−246.0	352.9	−370.2	−17.3	−40.8	2.2	−38.6

the hyperfine field at the Mn site is lower than the absolute value of the hyperfine fields at the copper and aluminium sites. It is important to note here the large negative value of the core contribution to the HFF at the Mn site. This can be quantitatively explained as follows. The majority-spin s electrons in the core will be pulled into the region of the spin-polarized 3d shell, since the exchange interaction is attractive, whereas the minority-spin electrons will be repelled from the 3d shell. At the Mn nuclear position an excess of minority-spin electrons, i.e., a negative polarization, is therefore created. Since Mn has a large moment (about 3.2 μ_B), the negative contribution to H_{val}(Cu) from the Mn moment is larger than the positive contribution from the Cu moment itself. Hence, the H_{val}(Cu) value becomes negative.

Furthermore, we see that the core contribution to the HFF at the Mn site is higher in the LSDA than in the GGA. If the local moment of the particular site increases, the core polarization will be large due to the exchange interaction of the polarized electrons with the s orbitals of the core. Hence, a higher value of the core contribution to the HFF at the Mn site for the LSDA than in the GGA can be understood in terms of the higher value of the local moment on the Mn site for the LSDA than in the GGA (table 1). Since the local moments on the copper and the aluminium sites are negligible, the core contribution to the HFF at these sites is small.

3. Total and partial density of states

We here calculated the total and the partial density of states of Cu_2MnAl utilizing the modified tetrahedron method of Blöchl *et al* [38]. Figure 5 shows the total density of states, where $\uparrow$ designates the majority-spin electrons and $\downarrow$ the minority-spin electrons. Here the region between −10 eV and −7 eV in the valence band is mainly due to the contributions from Al 3s states with small contributions also from Cu and Mn 4s states.

Decompositions of the total densities of states are given in figures 6 and 7, which show the majority-spin and the minority-spin d densities of states of Mn and Cu. An analysis of figures 6 and 7 reveals that the Cu 3d states are mainly confined to the 2–6 eV region of the valence band. This is consistent with the earlier-reported results from ultraviolet photoemission spectroscopy obtained by Brown *et al* [22]. In the experimental spectrum they observed a strong maximum at about 3.2 eV, dominated by contributions from the Cu 3d band, but our calculated results show that the main contribution of the Cu 3d band is at about 3.9 eV.

In their study they compared the experimental spectrum with the theoretical one obtained from the previous calculation using the symmetrized augmented-plane-wave method [13]. The comparison clearly shows a major difference between the experimental and the theoretical spectrum: unlike the experimental spectrum the theoretical one exhibits a peak at 1.5 eV, comprising contributions from both the Cu 3d and Mn 3d bands. In contrast, our calculated results shown in figure 6 and 7 do not exhibit any major peak at 1.5 eV below the Fermi level, supporting the experimental observation.

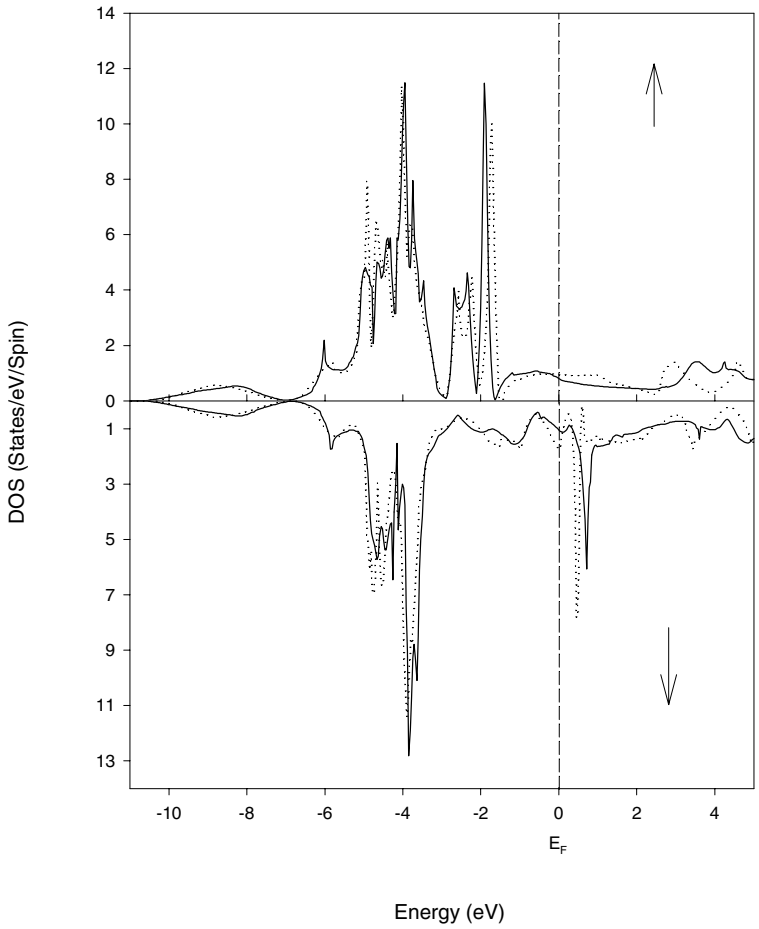

Figure 5. Total majority-spin (↑) and minority-spin (↓) densities of states per eV and unit cell for ferromagnetic Cu_2MnAl. The solid line and the dotted line represent the GGA and LSDA.

4. Electron densities

The electron-density maps were calculated for Cu_2MnAl in the [110] plane. The electron density is represented as a linear combination of real spherical harmonics inside the atomic spheres and as a Fourier series outside. A detailed calculation of charge densities within the FLAPW formulation is given by Blaha and Schwarz [39]. Figure 8 shows the electron density corresponding to the valence band.

Figure 9 shows the plot of the spin density ($\rho_\uparrow - \rho_\downarrow$) of Cu_2MnAl. The two strong peaks in figure 9 arise from the Mn atoms, thereby showing that the localized magnetization results from the exclusion of minority-spin electrons from the Mn 3d shell. It is important to note here that the magnitudes of the spin density around the copper atoms are very small.

5. Magnetic Compton profiles

The spin-dependent electron momentum densities are calculated in order to compare with the earlier-reported magnetic Compton profiles obtained by Zukowski *et al* [20]. Within

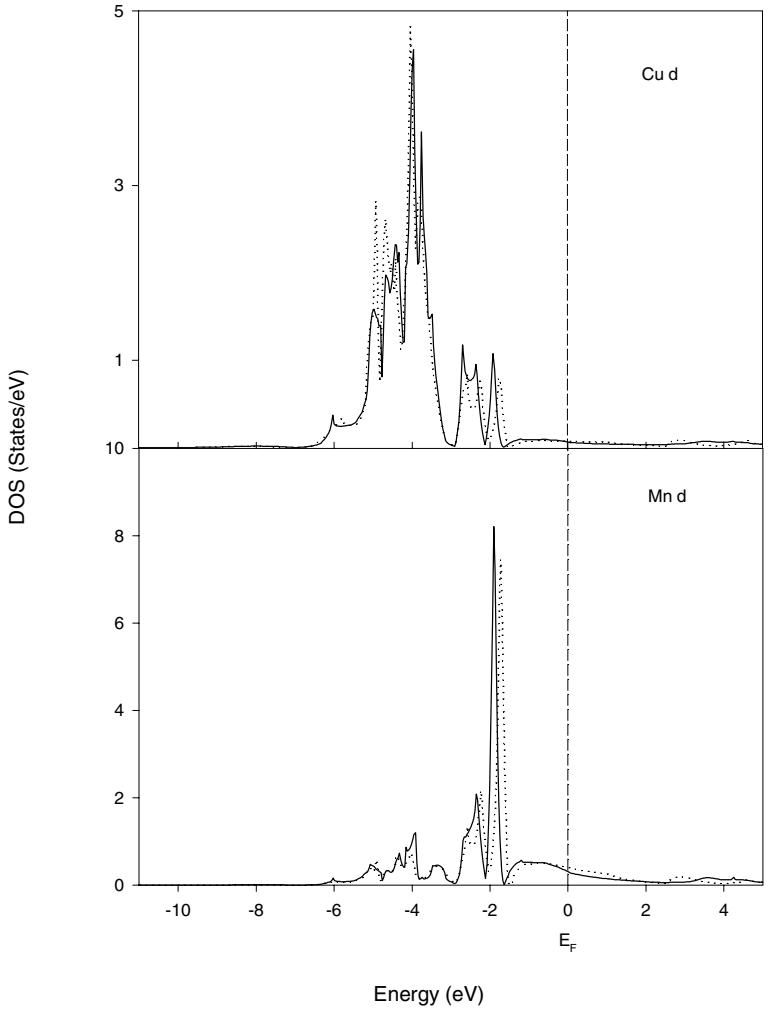

Figure 6. Majority-spin d-electron densities of states of Cu and Mn for ferromagnetic Cu_2MnAl. The solid line and the dotted line represent the GGA and LSDA.

the impulse approximation [40] the Compton profile, $J(p_z)$, is the projection of the electron momentum density, $n(\vec{p})$, along the scattering vector, which is conventionally defined as the z-axis:

$$J(p_z) = \int\int [n_\uparrow(\vec{p}) + n_\downarrow(\vec{p})]\,\mathrm{d}p_x\,\mathrm{d}p_y \tag{2}$$

where $n(\vec{p})$ is split into spin-up ($n_\uparrow(\vec{p})$) and spin-down ($n_\downarrow(\vec{p})$) components. $J_{mag}(p_z)$ is the spin-dependent momentum density, termed the magnetic Compton profile, and is a projection of the momentum distribution of the magnetic (unpaired spin) electrons, i.e.

$$J_{mag}(p_z) = \int\int [n_\uparrow(\vec{p}) - n_\downarrow(\vec{p})]\,\mathrm{d}p_x\,\mathrm{d}p_y. \tag{3}$$

Here, in both the FLAPW–LSDA and FLAPW–GGA schemes, the energy values and the wavefunctions are calculated at 512 k-points in the irreducible wedge of the Brillouin

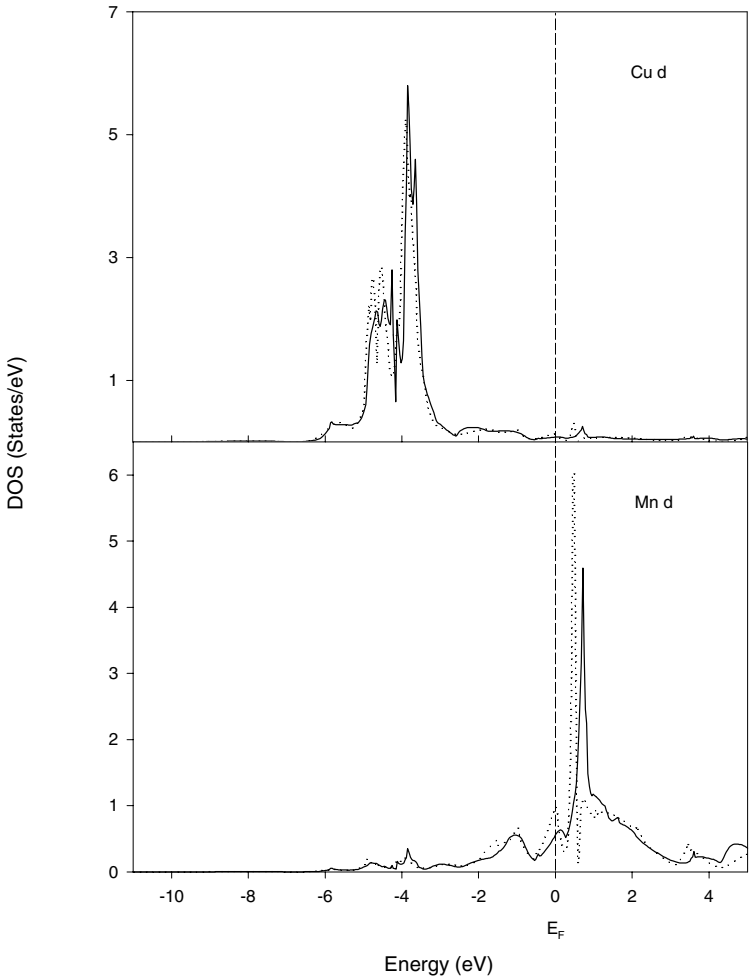

Figure 7. Minority-spin d-electron densities of states of Cu and Mn for ferromagnetic Cu_2MnAl. The solid line and the dotted line represent the GGA and LSDA.

zone. The momentum density of the band electrons is calculated using 1314 reciprocal-lattice vectors. The calculated magnetic Compton profiles along the [100], [110] and [111] directions are presented in figure 10, together with the experimental results of Zukowski *et al* [20]. The theoretical magnetic Compton profiles are convoluted with a Gaussian function of full width at half-maximum 0.5 atomic units (au) simulating the experimental resolution, and also normalized to the experimental moment of 2.86 μ_B as reported by Zukowski *et al* [20]. The present LSDA–FLAPW profiles show excellent agreements with those of the Korringa–Kohn–Rostoker (KKR) method based on the LSDA [20].

The FLAPW–GGA shows better agreement over the whole momentum region with the experiments than the FLAPW–LSDA for three directions. It is important to note that for the [100] direction there is a discrepancy between the experiment and the LSDA–FLAPW calculation for $p_z < 0.8$ au. This discrepancy is reduced for the GGA–FLAPW calculation, especially in the momentum region above 0.2 au. Below 0.2 au, however, the GGA also overestimates the momentum-density distribution of magnetic electrons.

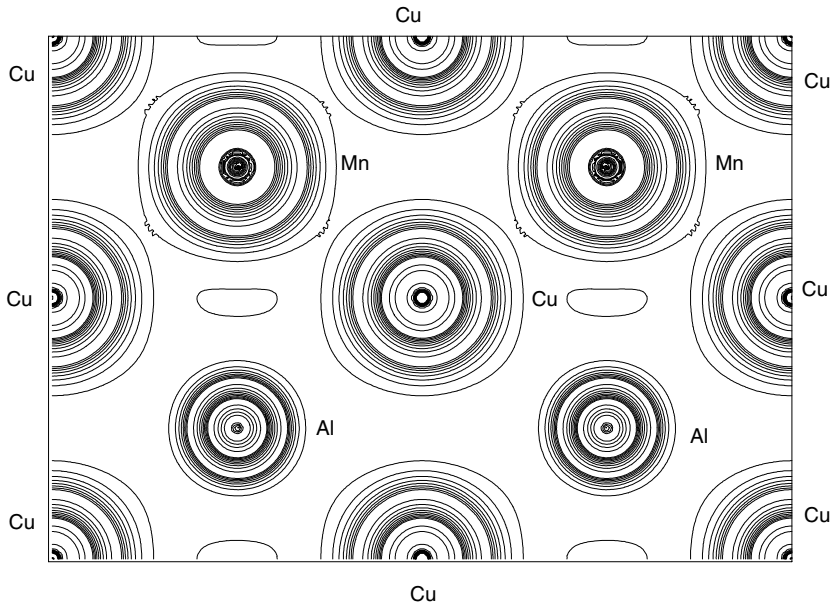

Figure 8. GGA–FLAPW valence electron density in the (110) plane in units of 0.01 electrons Å^{-3}; logarithmic scale; consecutive contour lines differ by a factor of $\sqrt{2}$.

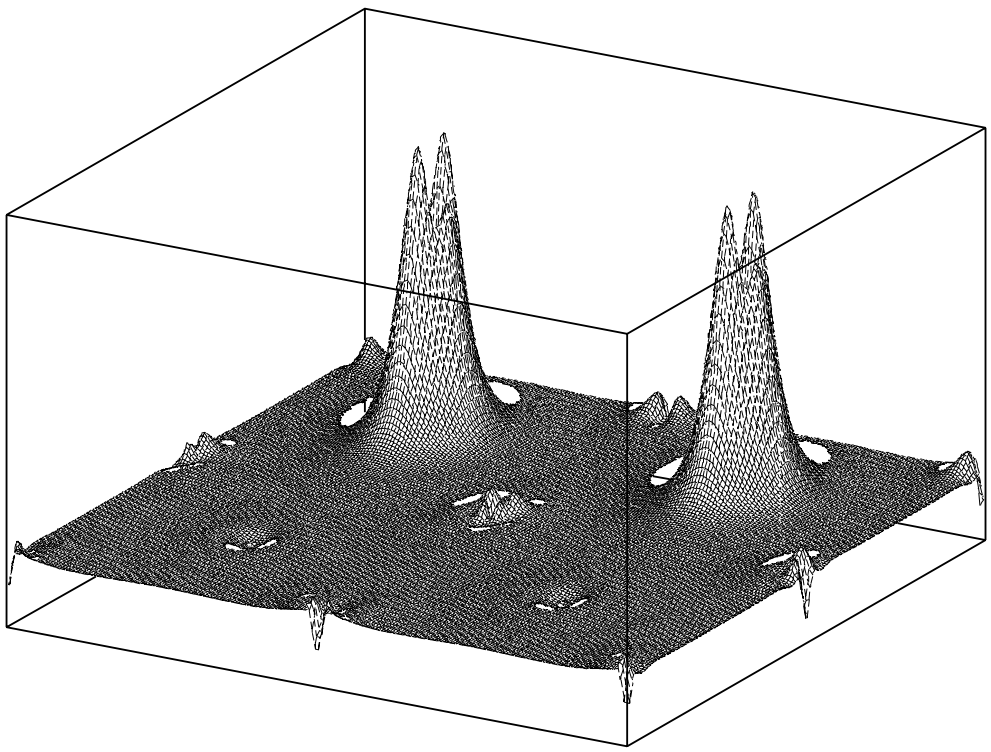

Figure 9. A GGA–FLAPW 3D plot of the spin density ($\rho_\uparrow - \rho_\downarrow$) of Cu_2MnAl in the (110) plane; linear scale, in units of electrons Å^{-3}.

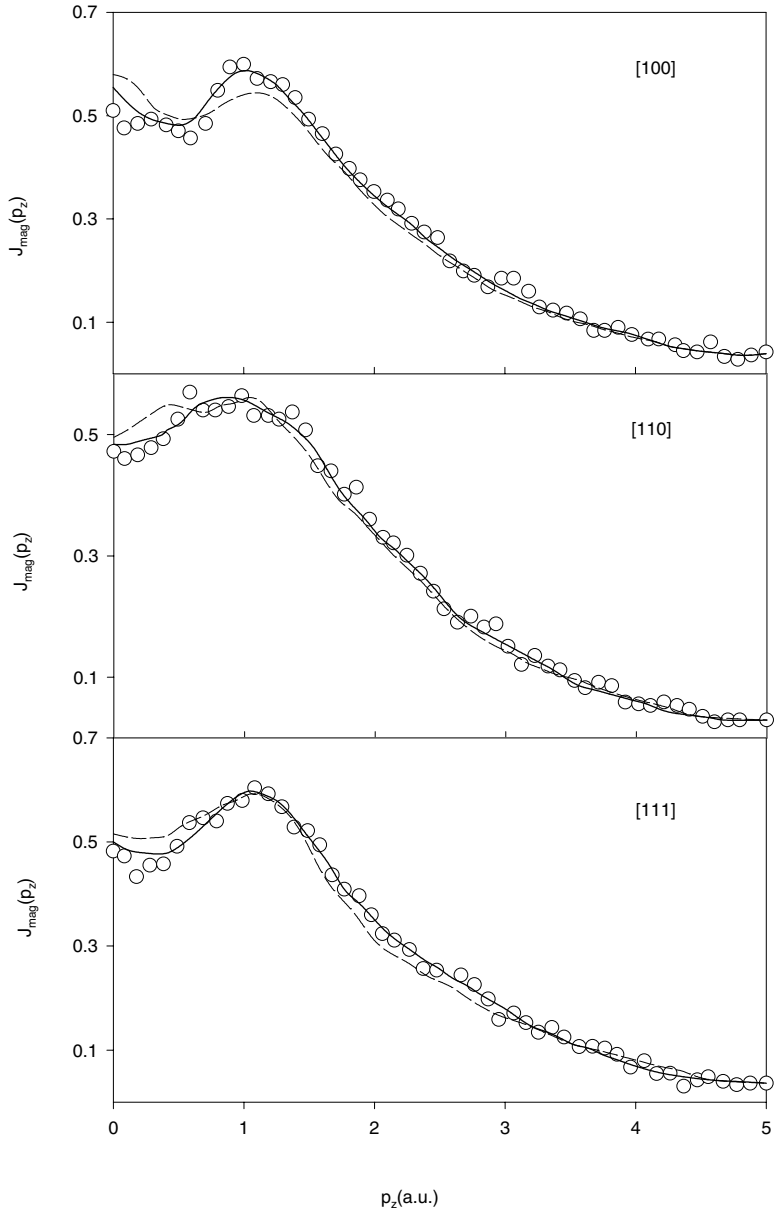

Figure 10. The theoretical and experimental directional spin-dependent (magnetic) Compton profiles of Cu_2MnAl. The key is as follows: solid line: GGA–FLAPW; dashed line: LSDA–FLAPW; open circles: experiment as reported by Zukowski *et al* [20]. The theoretical profiles have been convoluted with a Gaussian of FWHM $= 0.5$ au to represent the experimental resolution. Both the experimental and the theoretical (GGA–FLAPW and LSDA–FLAPW) results are normalized to the experimental moment of 2.86 μ_B [20].

6. Discussion and conclusions

We have carried out FLAPW energy band calculations utilizing the GGA and the LSDA scheme (figures 2 and 3) in order to study the electronic structure and bonding mechanism of Cu_2MnAl

Heusler alloy. We have studied the trends in spin moments, orbital moments and spin density and also calculated the hyperfine field. The hyperfine fields of Cu_2MnAl were calculated to examine the influence of surrounding magnetic atoms on the magnetic properties of an atom. We have seen that at the Mn site the valence and the core contribution are of opposite sign, resulting in a lower absolute value of the hyperfine field. It was also found that the core contribution at the Mn site was higher under the LSDA scheme than in the GGA, mainly because of the value of the local moment on the Mn site being higher for the LSDA than in the GGA. The self-consistent total energies calculated using the LSDA and GGA functionals are given in table 1. The total energy calculated with the GGA functional is found to be less than the total energy within the LSDA scheme. The band-structure-character plots in figures 4(a)–4(d) provide a clear idea of the contributions of the different states of Cu and Mn in the valence and the conduction bands for the majority and the minority spins respectively. It is found that the localized character of the magnetization results from the exclusion of the minority-spin electrons from the Mn 3d shell. Thus our calculation provides further concrete proof of the results stated earlier by Kübler *et al* [18].

The Mn 3d and Cu 3d contribution to the density of states extends to 6 eV below the Fermi level, which is in agreement with the theoretical results of Kübler *et al* [18], based on the LSDA treatment of electronic exchange and correlation and on the augmented-spherical-wave method. Consistent with the earlier-reported experimental results obtained by Brown *et al* [22], our calculated state densities for Cu 3d each show a peak at approximately 3.9 eV. More importantly, in our calculated results the Cu 3d band and the Mn 3d band did not exhibit any major peak at 1.5 eV in the valence band (figures 6 and 7), while the previous calculation [13] gives a peak. Our calculation is consistent with the experimental findings of Brown *et al* [22].

On the other hand, we have seen here that the localized character of the magnetization results from the exclusion of the minority-spin electrons from the Mn 3d shell (from figures 6, 7 and 9), and the 3d spin moment of 3.20 μ_B on the Mn site in the GGA scheme is in close agreement with the experimental values of Zukowski *et al* [20] and with the value of 3.21 μ_B obtained by the earlier neutron experiments. It is also important to note here that within the LSDA scheme our calculated 3d spin moment on the Mn site is close to the calculated value reported by Kübler *et al* [18], both being higher than the recent experimental value of Zukowski *et al* [20] (table 1).

The magnetic Compton profiles from the GGA–FLAPW calculations agree with the experiments better than the LSDA–FLAPW calculations. Compared with the LSDA–FLAPW calculation, the GGA–FLAPW one shows higher momentum density above 0.8 au, but lower density below it. That is, the GGA–FLAPW calculation gives more localized Mn 3d majority-spin electrons in real space—while they are delocalized in momentum space—than the LSDA–FLAPW one. This is consistent with a finding from figure 2, where the GGA–FLAPW calculation has a deeper Mn 3d majority-spin band around -2 eV than the LSDA–FLAPW one. The GGA–FLAPW calculation also produces a value for the spin moment closer to the accepted experimental value. It is seen from the GGA–FLAPW calculations that there is no magnetic contribution from the Cu site, again in agreement with the Compton scattering data.

So far we have shown that the GGA can reproduce satisfactorily most of the earlier-reported experimental observations. Therefore we believe that the present calculation firmly substantiates the assertion that GGA works well for the 3d Heusler alloy, Cu_2MnAl, in the same way as for 3d transition metals [32, 41, 42].

Finally, from our study of the magnetic Compton profiles, it is evident that the GGA improves on the LSDA at momenta below 1 au. From an experimental point of view, high-resolution measurements [43–47] ($\triangle p \approx 0.15$ au, achievable with a crystal spectrometer)

would now be useful in order to investigate specific features in these profiles which are not well described, i.e. the shapes of the profiles at low momentum and the blurring of the Umklapp features.

Acknowledgments

The authors would like to thank Professor Shiotani and Professor Kubo for helpful discussions and acknowledge the support by the SPring-8 Joint Research Promotion Scheme under the auspices of Japan Science and Technology Agency.

References

[1] Villiars P and Calvert L D 1985 *Pearson's Handbook of Crystallographic Data for Intermetallic Phases* vol 2 (Metals Park, OH: American Society for Metals)
[2] Webster P J and Ramadan M R I 1979 *J. Magn. Magn. Mater.* **13** 301
[3] Webster P J 1968 *PhD Thesis* University of Sheffield
[4] *Landolt–Börnstein New Series* 1988 Group III, vol 19c (Berlin: Springer) pp 75–185
[5] Oxley D P, Tebble R S and Williams K C 1963 *J. Appl. Phys.* **34** 1362
[6] Kozubski R and Soltys J 1982 *J. Mater. Sci.* **17** 1441
[7] Sakka Y and Nakamura M 1990 *J. Mater. Sci.* **25** 2549
[8] Soltys J, Stefaniak M and Holender J 1984 *Phil. Mag.* B **49** 151
[9] Felcher G P, Cable J W and Wilkinson M K 1963 *J. Phys. Chem. Solids* **24** 1663
[10] Ishikawa Y 1977 *Physica* B **91** 130
[11] Tajima K, Ishikawa Y, Webster P J, Stringfellow M W, Tocchetti D and Ziebeck K R A 1977 *J. Phys. Soc. Japan* **43** 483
[12] Noda Y and Ishikawa Y 1976 *J. Phys. Soc. Japan* **40** 699
[13] Ishida S, Ishida J, Asano S and Yamashita J 1978 *J. Phys. Soc. Japan* **45** 1239
[14] Tobala J, Pierre J, Kaprzyk S, Skolozdra R V and Kouacou M A 1996 *J. Magn. Magn. Mater.* **159** 192
[15] Kübler J 1984 *Physica* B **27** 257
[16] Fujii S, Sugimura S, Ishida S and Asano S 1990 *J. Phys.: Condens. Matter* **2** 8583
[17] Williams A R, Moruzzi V L, Gelatt C D Jr and Kübler J 1983 *J. Magn. Magn. Mater.* **31–34** 88
[18] Kübler J, Williams A R and Sommers C B 1983 *Phys. Rev.* B **28** 1745
[19] Ishida S, Kubo Y, Ishida J and Asano S 1980 *J. Phys. Soc. Japan* **48** 814
[20] Zukowski W, Andrejczuk A, Dobrzynski L, Cooper M J, Dixon M A G, Gardelis S, Lawson P K, Buslaps T, Kaprzyk S, Neumann K U and Ziebeck K R A 1997 *J. Phys.: Condens. Matter* **9** 10 993
[21] Rakchecha V C, Chakraborty R and Satya Murthy N S 1976 *Proc. Conf. on Neutron Scattering (Gatlinburg, TN, 1976)* vol 2, p 638
[22] Brown D, Crapper M D, Bedwell K H, Flannery L B, Petty M and Skull P A 1996 *J. Phys.: Condens. Matter* **8** 5941
[23] Blaha P, Schwarz K, Sorantin P and Tricky S B 1990 *Comput. Phys. Commun.* **59** 399
[24] Pickett W E 1985 *Comment. Solid State Phys.* **12** 1
[25] Perdew J P 1991 *Physica* B **172** 1
[26] Bagno P, Jepsen O and Gunnarsson O 1989 *Phys. Rev.* B **40** 1997
[27] Barbiellini B, Moroni E G and Jarlborg T 1990 *J. Phys.: Condens. Matter* **2** 7597
[28] Hammer B, Scheffler M, Jacobsen K W and Norskov J K 1994 *Phys. Rev. Lett.* **73** 1400
White J A, Bird D M, Payne M C and Stich I 1994 *Phys. Rev. Lett.* **73** 1404
[29] Ortiz G and Ballone P 1991 *Phys. Rev.* B **43** 6376
[30] Perdew J P, Chevary J A, Vosko S H, Jackson K A, Pederson M R, Singh D J and Fiolhais C 1992 *Phys. Rev.* B **46** 6671
[31] Lee In Ho and Martin R M 1997 *Phys. Rev.* B **56** 7197
[32] Kokko K and Das M P 1998 *J. Phys.: Condens. Matter* **10** 1285
[33] Perdew J P and Wang Y 1992 *Phys. Rev.* B **45** 13 244
[34] Bozorth R M 1951 *Ferromagnetism* (New York: Van Nostrand)
[35] Dunlap R A, Stroink G and Dini K 1986 *J. Phys. F: Met. Phys.* **16** 1083
[36] Endo K, Phayama T and Kitamura R 1964 *J. Phys. Soc. Japan* **19** 1494
[37] Blügel S, Akai H, Zeller R and Dederichs P H 1994 *Phys. Rev.* B **49** 10 170

[38] Blöchl P E, Jepsen O and Anderson O K 1994 *Phys. Rev.* B **49** 16 223
[39] Blaha P and Schwarz K 1983 *Int. J. Quantum Chem.* **23** 1535
[40] Platzman P M and Tzoar N 1970 *Phys. Rev.* B **2** 3556
[41] Singh D. J, Pickett W E and Krakauer H 1991 *Phys. Rev.* B **43** 11 628
[42] Leung T C, Chan C T and Harmon B N 1991 *Phys. Rev.* **44** 2923
[43] Cooper M J 1985 *Rep. Prog. Phys.* **48** 415
[44] Sakurai Y, Tanaka Y, Bansil A, Kaprzyk S, Stewart A T, Nagashima Y, Hyodo T, Nanao S, Kawata H and Shiotani N 1995 *Phys. Rev. Lett.* **74 2252**
[45] Schülke W, Stutz G, Wohlert F and Kaprolat A 1996 *Phys. Rev.* B **54** 14 381
[46] Hämäläinen K, Manninen S, Kao C C, Caliebe W, Hastings J B, Bansil A, Kaprzyk S and Platzman P M 1996 *Phys. Rev.* B **54** 5453
[47] Kaprzyk S 1997 *Acta Phys. Pol.* A **91** 135